Available online at www.sciencedirect.com
ScienceDirect
Trans. Nonferrous Met. Soc. China 35(2025) 143−156
Transactions of Nonferrous Metals Society of China
www.tnmsc.cn

Corrosion resistance and antibacterial properties of Ti−3Cu alloy prepared by selective laser melting

Meng-zhen ZHU[1], Jing-lei MIAO[2], Xiong-wen ZHOU[3], Er-lin ZHANG[4], Zhi-lin LIU[5], Hai-lin YANG[1]

1. State Key Laboratory of Powder Metallurgy, Central South University, Changsha 410083, China;
2. The Third Xiangya Hospital, Central South University, Changsha 410013, China;
3. Department of Prosthodontics, Centre of Stomatology, Xiangya Hospital, Central South University, Changsha 410008, China;
4. Key Laboratory for Anisotropy and Texture of Materials, Ministry of Education, School of Materials Science and Engineering, Northeastern University, Shenyang 110819, China;
5. Light Alloy Research Institute, College of Mechanical and Electrical Engineering, Central South University, Changsha 410083, China

Received 29 May 2023; accepted 21 December 2023

Abstract: The corrosion resistance and antibacterial properties of Ti−3Cu alloy prepared by selective laser melting were evaluated using electrochemical experiments and a variety of antibacterial characterization. It is found that the charge transfer resistance of Ti−3Cu alloy was 4.89×10^5 Ω·cm^2, which was doubled the data obtained by CP-Ti alloy. The antibacterial rates of Ti−3Cu alloy against *S. mutans* and *P. gingivalis* were 45.0% and 54.5%. And the antibacterial rates increased with the prolongation of cultivation time, reaching up to 62.8% and 68.6%, respectively. The in-situ nano Ti_2Cu precipitates were homogeneously distributed in the matrix of the Ti−3Cu alloy, which was the key reason of increasing the corrosion resistance. Additionally, the microscale electric fields between the α-Ti matrix and the Ti_2Cu was responsible for the enhancement of the antibacterial properties.

Key words: selective laser melting; Ti−3Cu alloy; microstructure; corrosion resistance; antibacterial properties

1 Introduction

Titanium and its alloys have been widely used for artificial dental implants because of the remarkable advantages of low acquisition cost, excellent corrosion resistance, and good biocompatibility [1−3]. Although commercial pure titanium delivers good biocompatibility, the postoperative infection usually occurs due to the bacterial proliferation on the dental implant and enamel surface [4−6]. Moreover, the biofilm on the implant often induces inflammation in the tissues around the CP-Ti implant, and the occurrence of peri-implant inflammation even results in surgical failure or reoperation [7,8]. Therefore, the materials or processing approaches that can eliminate these problems are attractive for materials scientist and biological scientists.

Copper (Cu) element is a broad-spectrum antibacterial element. A trace of Cu is also the basis of many physiological functions in the human body [9]. It is reported that the Ti−3Cu alloy retains good biocompatibility [10]. Meanwhile, the alloy

Corresponding author: Hai-lin YANG, Tel: +86-13973182703, E-mail: y-hailin@csu.edu.cn;
Jing-lei MIAO, Tel: +86-13787056928, E-mail: miaojinglei@126.com;
Xiong-wen ZHOU, Tel: +86-13707310367, E-mail: zhouxw1128@csu.edu.cn

https://doi.org/10.1016/S1003-6326(24)66670-7

design strategy of titanium alloys or stainless steel with a trace of Cu addition is conducive to antibacterial performance [11−13]. For instance, the Ti−5Cu alloy is capable of offering a strong inhibitory activity on the formation of biofilms of *Staphylococcus aureus* and *Escherichia coli* [14]. It is also noted that the addition of Cu into Ti−6Al−4V alloy can simultaneously improve the mechanical and antibacterial properties [11,13,15]. Hence, tuning the addition amount of Cu can guarantee the superior antibacterial and mechanical properties of titanium alloys [16,17].

The widely used Ti−3Cu alloy possesses good biocompatibility, antibacterial performance, excellent mechanical properties and corrosion resistance [7,10]. In the Ti−3Cu alloy, Cu usually exists in the form of solid solution and precipitates. The size of precipitates fabricated via conventional handicrafts is at a level of micron or submicron [18−20]. The occurrence of inflammation usually goes through the process of bacterial adhesion and biofilm formation on the surface of dental implants. *S. mutans* and *P. gingivalis* are two important bacteria in the biofilm formation on the surface of dental implants, which have a significant impact on promoting biofilm formation and inflammatory response. Although the nano-sized copper-bearing precipitates on the mechanical properties of Ti−Cu alloy have been fully investigated, the antibacterial performance of *S. mutans* and *P. gingivalis* of the conventionally prepared Ti−Cu alloys was not excellent, and thus the improvement for the alloy composition or the manufacturing approaches is still necessary to satisfy the real requirement in applications.

Metal-based additive manufacturing (AM) has enabled the fabrication of near net shape metal components with optimized geometries that are not achievable through conventional manufacturing techniques [21,22]. The Ti−6Al−4V alloy fabricated via selective laser melting exhibits better corrosion resistance [23]. The refined matrix grain and ultrafine precipitates have been achieved when solidification with a high cooling rate, and it delivers excellent mechanical properties [24]. Also, a high number density of homogeneously distributed ultrafine Ti_2Cu precipitates in the Ti−3Cu alloy have potential to result in good antibacterial ability [19]. Additionally, metals are more likely prone to acid erosion in the oral with a highly humid environment, and certain metal ions released to human body could inhibit the solidification of proteins and the activation of related enzymes [25,26]. Therefore, it is expected that the AM method can be applied to the Ti−3Cu alloy for improved antibacterial and electrochemical properties. As such, the present work focuses on the selective laser melting (SLM) of the Ti−3Cu alloy. The microstructural features were examined and the antibacterial properties and electrochemical properties were studied in association with the microstructure. And the corrosion resistance principle and the possible antibacterial mechanisms of the Ti−3Cu alloy processed via SLM were discussed.

2 Experimental

2.1 Material preparation

CP-Ti (Grade 2) was used as the reference group. The pre-alloyed Ti−3Cu powder for SLM process was prepared through electrode induction melting gas atomization with the particle size of 15−53 μm. SLM process was performed in a FS271 (Farsoon, Inc., China) machine equipped with a 200 W ytterbium fiber laser. The optimized parameters were set with a laser power (P) of 200 W, a scan speed (v) of 1000 mm/s, a layer thickness (t) of 30 μm, a hatch spacing (h) of 100 μm, and a scan rotation angle of 67° between successive layers. To ensure that the two groups of alloys had the same surface state before the subsequent test, the alloys were ground using $400^{\#}$−$2000^{\#}$ SiC paper and then polished with OPS solution.

2.2 Microstructure characterization

Phase analysis was conducted by X-ray diffractometer (XRD, DX-2700B). The microstructure was detected with optical microscope (OM, DM2700M), scanning electron microscope (SEM, MTEST2000) and transmission electron microscope (TEM, Talos F200X). Particle sizes and morphology of precipitates were then determined using high-angle annular dark fields image and energy-dispersive X-ray spectroscopy mapping. Prior to TEM observation, the sample was thinned using the precision ion polishing system (PIPS) at a voltage of 5 kV/2 kV and an incident angle of 3°−7°.

2.3 Electrochemical test

Electrochemical experiments were performed on the polished alloys in 1000 mL sodium chloride solution with a mass fraction of 0.9% using CHI660D equipment. When the open circuit voltage was stable, the polarization curve was tested to investigate the passivation behaviour and corrosion rate. The scanning speed was 10 mV/s, and the initial potential and termination potential were −1.6 and 0 V, respectively. Then, the electrochemical impedance spectroscopy (EIS) curve was obtained by applying small amplitude sine waves of different frequencies to the three-electrode system. The sinusoidal AC voltage was set at 10 mV, and the scanning frequency range was 0.1−100 kHz. ZView software was used to design the equivalent circuit and fit the EIS results.

2.4 Physicochemical properties test

According to the GB/T 16886.12 — 2017 standard, the Ti−3Cu alloy was isothermally immersed at 37 °C in 0.9 wt.% NaCl solution for time ranging from 6 to 72 h, followed by Cu^{2+} released measurement. And the concentrations of released Cu^{2+} were determined using inductively coupled plasma atomic emission spectrometry (ICP-AES, iCAP7600). The drop shape analyzer (DCA100) was employed to measure the surface contact angles. The wettability was evaluated by the sessile drop method and all the measurements were conducted at ambient temperature using the deionized water and plasma as wetting liquids.

2.5 Antibacterial assessment

Throughout the antimicrobial performance test, the cell was cultured at a constant temperature ((37±1) °C) under the conditions of 5% CO_2 and 90% relative humidity. The frozen powder of *S. mutans* ATCC 25175 and *P. gingivalis* ATCC 33277 was dissolved in the culture medium, followed by constant temperature culture. After culture, the bacterial suspensions were diluted to 1×10^6 CFU/mL.

Inhibition zone assay was performed on polished samples to establish the antibacterial activity. After being co-cultured with agar for 24 h, the size of antibacterial ring was measured and counted. The quantitative antibacterial test was carried out according to the standard test method of GB/T 2519. The colony forming units (CFU) at each dilution rate were counted according to the Chinese National Standard GB/T 4789.2 — 2010. Subsequently, the average was determined, and the total number of bacteria was calculated according to dilution. Finally, the colony number of CP-Ti co-cultured under the same conditions was selected as the control group to calculate and evaluate the bactericidal capacity of Ti−3Cu alloy. The calculation formula is as follows:

$$R=(N_1-N_2)/N_1\times100\% \quad (1)$$

where R is the antibacterial rate, and N_1 and N_2 represent the average amounts of bacteria colonies on Ti−3Cu and CP-Ti, respectively.

Field emission scanning electron microscope (FE-SEM, S-3400N) was used to observe the morphology of bacteria and determine the formation of bacterial biofilm after 24 h isothermal co-culture. To further observe the variation of bacterial activity and bacterial biofilm with the prolongation of cultivation time, the samples were stained with LIVE/DEAD® Bacterial™ Viability Kits L7012 at 24 and 72 h, respectively. Subsequently, staining results were observed under a fluorescence microscope (Leica DMi8) immediately. The level of intracellular reactive oxygen species (ROS) was investigated by measuring the fluorescent intensity of the dichlorofluorescein probe. Firstly, the samples were stained with the 2’7’-dichlorodihydrofluorescein diacetate (DCFH-DA, Beyotime) for 0.5 h and the excess dye was washed away. Then, the samples were observed under fluorescence microscope (Leica DMi8) to detect the ROS level.

2.6 Statistical analysis

T test was used to evaluate the difference between the groups using SPSS 23.0 software for Windows (SPSS Inc., USA). Three parallel samples were prepared before every experiment. And at least three measurements were performed to obtain the average value and the mean standard deviation. A p-value of less than 0.05 was considered statistically significant.

3 Results

3.1 Structure

The XRD pattern and microstructure of the as-SLMed Ti−3Cu alloy is shown in Fig. 1. The

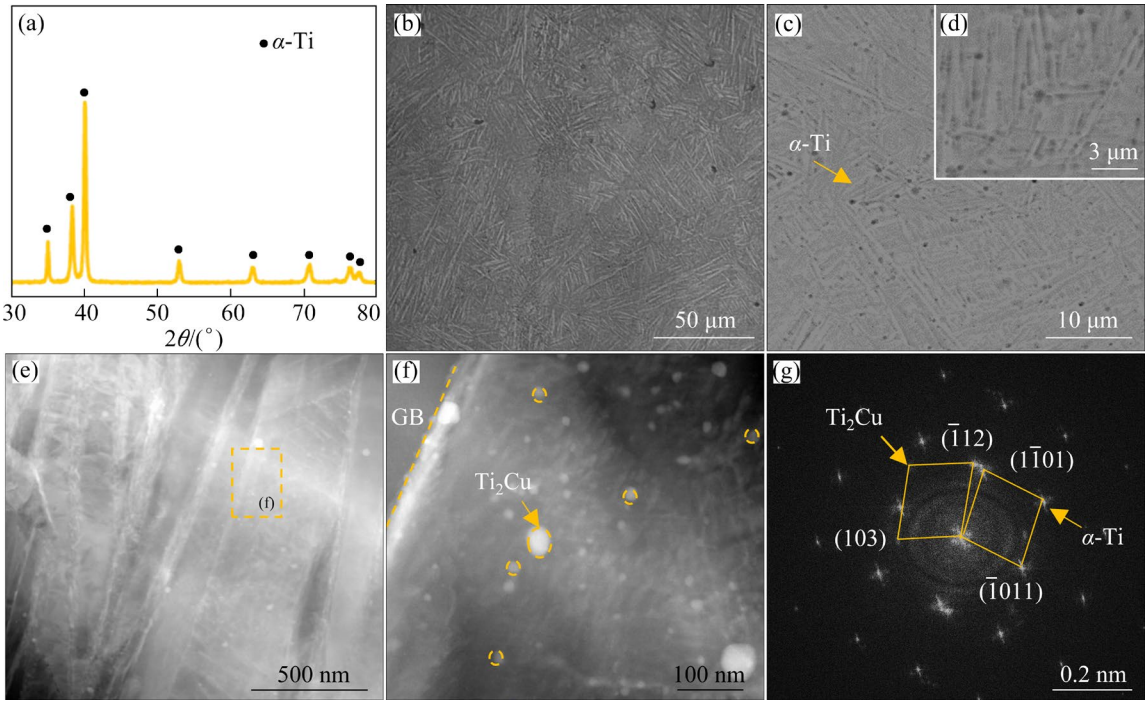

Fig. 1 Microstructure characterization of Ti−3Cu alloy: (a) XRD pattern; (b) Optical micrograph (OM); (c, d) SEM images; (e−g) HAADF-STEM images and corresponding SAED pattern

diffraction peak of α-Ti could be obviously observed, but the diffraction peak of Ti_2Cu was difficult to distinguish (Fig. 1(a)). This was likely due to the low level of Cu addition. Figures 1(b−d) showed that the α-Ti matrix exhibited a fine needle-like morphology. It was well documented that the Ti_2Cu nano-precipitates could be induced in the supersaturated Ti−3Cu alloy during subsequent thermal cycling of layer-by-layer scanning of SLM manufacturing. Correspondingly, a low magnification HAADF-STEM image of the fine needle-like grain region is shown in Fig. 1(e). Nano-sized precipitates were detected both within the grains and at the grain boundaries. The white particles with a size of 10−50 nm in Fig. 1(e) were identified as Ti_2Cu.

3.2 Corrosion performance

The potentiodynamic anodic polarization curves are shown in Fig. 2(a). It is seen that no obvious passivation region was found in the polarization curves. The self-corrosion potential (φ_{corr}) and self-corrosion current density (J_{corr}) obtained after Tafel analysis are given in Table 1. The φ_{corr} of Ti−3Cu alloy and CP-Ti alloy were −0.99 and −1.07 V, while the J_{corr} of Ti−3Cu alloy and the CP-Ti alloy were 2.81×10^{-7} A/cm^2 and 3.56×10^{-7} A/cm^2, respectively. The slightly higher φ_{corr} and lower J_{corr} suggested that the corrosion tendency and corrosion rate of Ti−3Cu alloy were smaller than those of the CP-Ti. The equivalent circuit $R(QR)$ with only one time constant representing the impedance spectrum is shown in Fig. 2(c). In Table 2, the solution resistance values of two groups of samples were roughly the same, while the charge transfer resistance of CP-Ti (2.20×10^5 Ω·cm^2) was far less than that of the Ti−3Cu (4.89×10^5 Ω·cm^2), which implied that the as-SLMed Ti−3Cu alloy had lower corrosion rate. These impedance parameters also demonstrated that a highly compacted passive Ti oxide film was formed on the CP-Ti and the Ti−3Cu [27]. And it was likely that a more stable passive film was formed in the Ti−3Cu alloy, which behaved as an efficient barrier to corrosion and increased the resistance to charge transfer at the electrolyte/oxide layer interface.

3.3 Physicochemical properties

In Fig. 3(a), the Cu^{2+} amount released within 24 h was 53.3 μg/L and the release rate decreased gradually with the prolongation of the incubation time. Figure 3(b) shows the comparison of the contact angle on the CP-Ti and Ti−3Cu. The contact

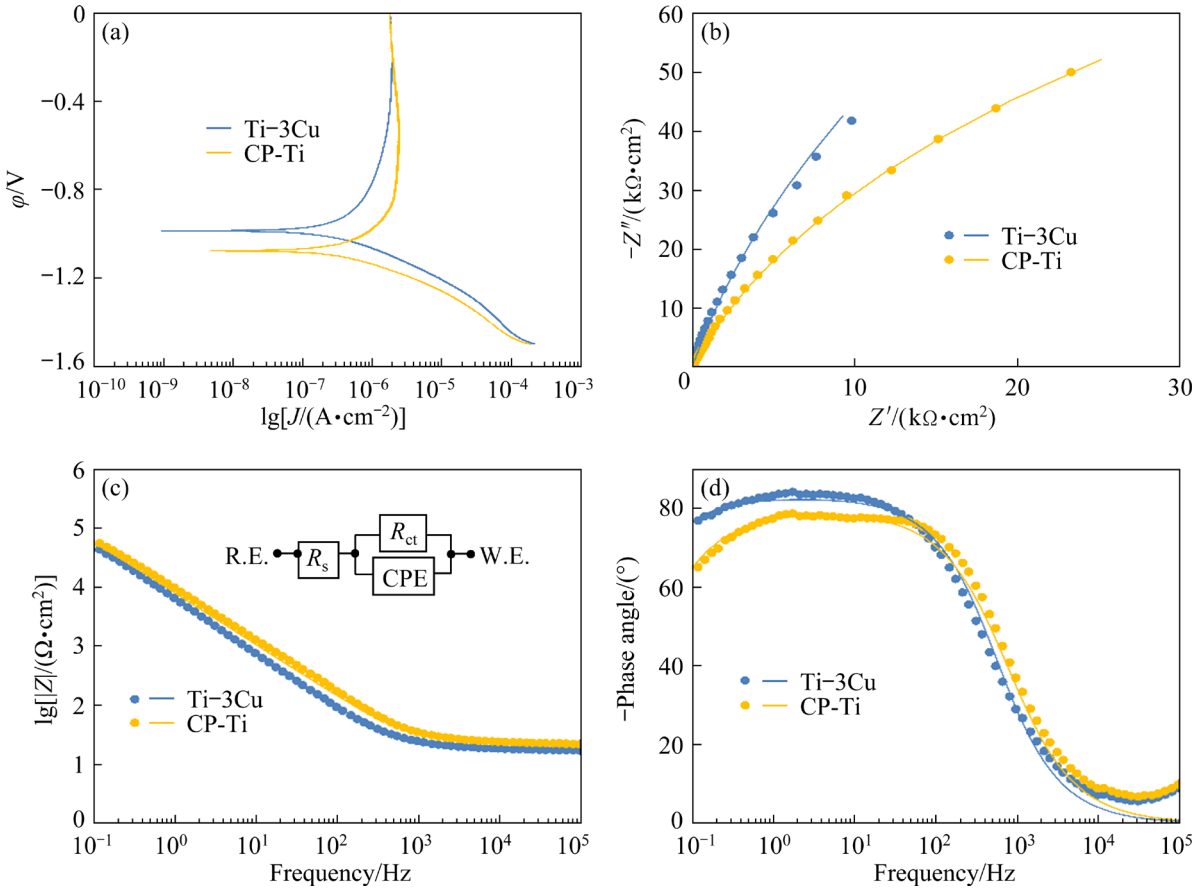

Fig. 2 Electrochemical measurement results for CP-Ti and Ti−3Cu alloy at 25 °C in 0.9 wt.% NaCl: (a) Potentiodynamic polarization curves; (b) Nyquist plot; (c, d) Bode plots (R_s is the solution resistance, R_{ct} is the charge transfer resistance, and CPE is the constant phase element)

Table 1 Tafel analysis results from potentiodynamic polarization curves of CP-Ti and Ti−3Cu alloys in 0.9 wt.% NaCl solution tested at 25 °C

Sample	φ_{corr}/V	J_{corr}/(A·cm^{-2})
CP-Ti	−1.07	3.56×10^{-7}
Ti−3Cu	−0.99	2.81×10^{-7}

Table 2 EIS fitting results of CP-Ti and Ti−3Cu alloys in 0.9 wt.% NaCl solution with equivalent circuit

Sample	R_s/(Ω·cm^2)	R_{ct}/(Ω·cm^2)	CPE/(F·cm^{-2})	n
CP-Ti	22.78	2.20×10^5	2.07×10^{-5}	0.88
Ti−3Cu	18.20	4.89×10^5	2.96×10^{-5}	0.92

angle of CP-Ti and Ti−3Cu in water were basically identical, which was about 40°. However, the plasma contact angle of Ti−3Cu was obviously smaller in comparison with that of CP-Ti, indicating that the Ti−3Cu alloy offered the better hydrophilicity.

3.4 Antibacterial activity

The ability of CP-Ti and Ti−3Cu to prevent bacteria growth was examined through inhibition zone assay. In Fig. 4, the same inhibition ring diameters of 11.8 mm on *S. mutans* and *P. gingivalis* were acquired after 24 h isothermally co-cultured with CP-Ti, while the inhibition ring diameters of Ti−3Cu on *S. mutans* and *P. gingivalis* were 14 and 13.6 mm, respectively. Compared with the CP-Ti, the Ti−3Cu alloy could effectively inhibit the growth of bacteria in the contact area of agar plate, confirming that the Ti−3Cu alloy had significantly antibacterial activity against both bacteria species.

Bulk samples were isothermally co-cultured with *S. mutans* and *P. gingivalis* for 24−72 h at 37 °C to further determine the antibacterial rate for the Ti−3Cu. In Figs. 5(a, b), Ti−3Cu alloy showed a significant reduction in colony-forming unit (CFU) in both bacteria species at both time points compared to the CP-Ti. Furthermore, the number of

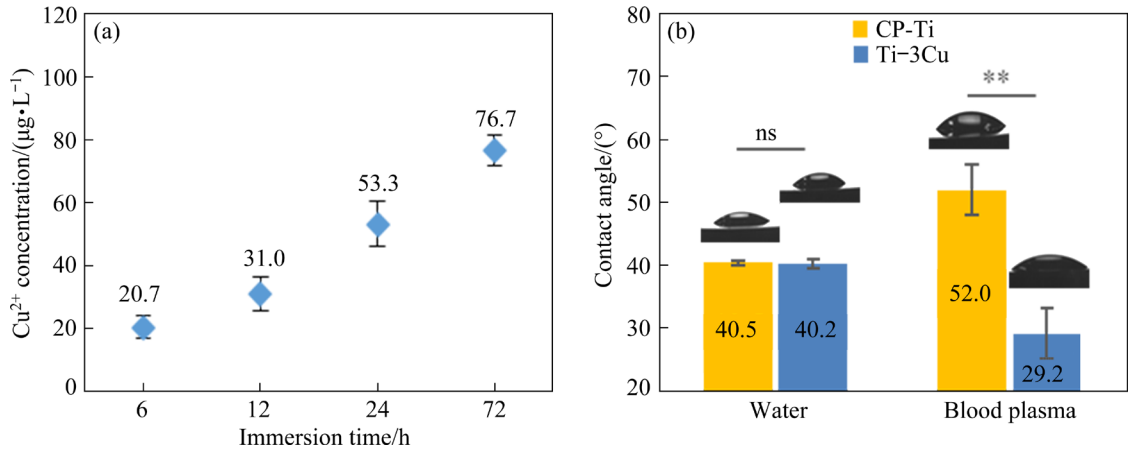

Fig. 3 Physicochemical properties: (a) Cumulative Cu^{2+} concentration released from Ti−3Cu alloy in 0.9 wt.% NaCl solution; (b) Comparison of contact angles with water and blood plasma on CP-Ti and Ti−3Cu alloys ("ns" represents no significantly difference; **p<0.01, compared to CP-Ti)

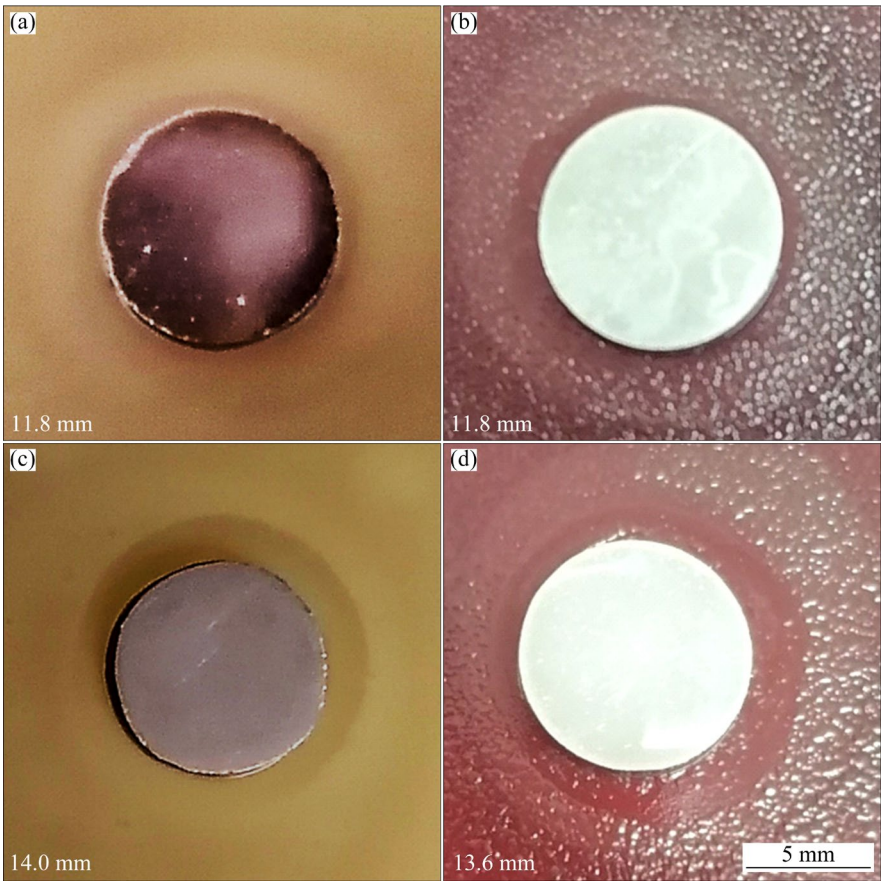

Fig. 4 Typical images of inhibition zones on CP-Ti (a, b) and Ti−3Cu (c, d) disks of *S. mutans* (a, c) and *P. gingivalis* (b, d) co-cultured with agar for 24 h

surviving bacteria colonies distributed on the CP-Ti basically remained no obvious change with extending the cultivation time to 72 h. However, the number of surviving bacteria colonies distributed on the Ti−3Cu decreased significantly with the culture time extension. Furthermore, only scattered colonies could be detected on the Ti−3Cu after the cultivation for 24 and 72 h (Figs. 5(c−f)). Table 3 shows the antibacterial rates of Ti−3Cu at different incubation time. Under the condition of 24 h cultivation, the antibacterial rates of 45.0% against *S. mutans* and 54.5% against *P. gingivalis* of the

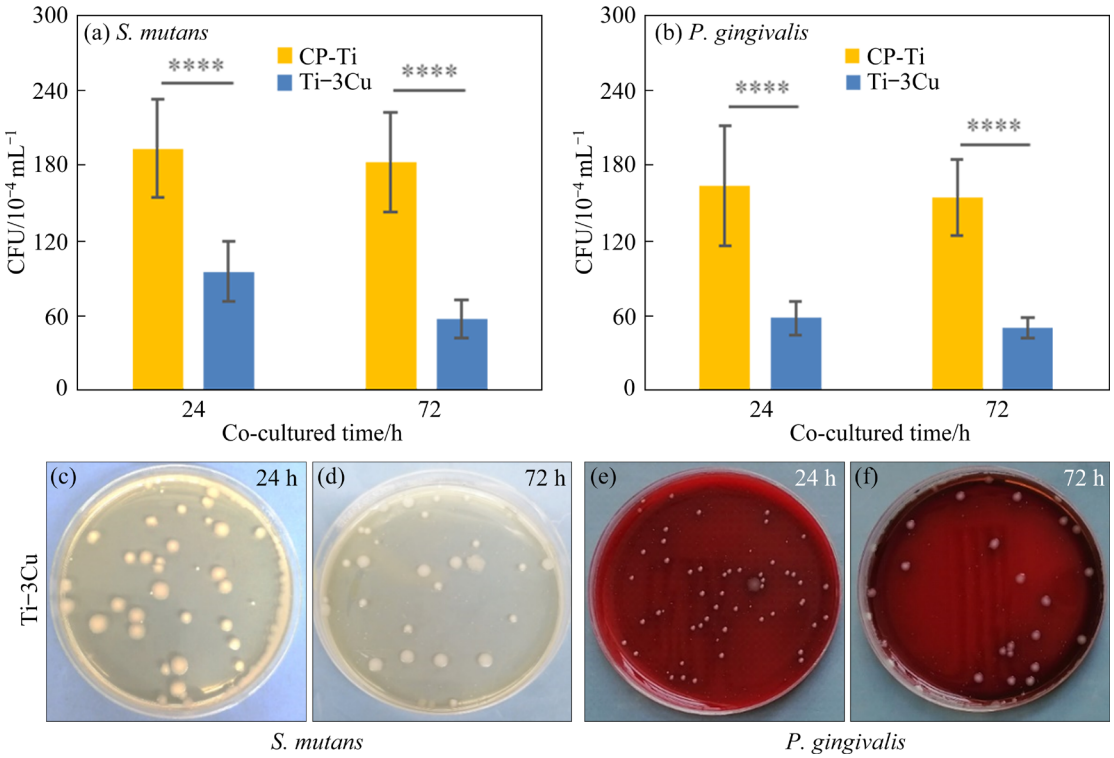

Fig. 5 Quantitative antibacterial behaviour evaluation of CP-Ti and Ti−3Cu alloys: (a, b) Concentration of *S. mutans* and *P. gingivalis* versus co-cultured time (****p<0.0001); (c−f) Typical colonization images of *S. mutans* and *P. gingivalis* after being co-cultured with Ti−3Cu alloy

Table 3 Antibacterial rates of Ti−3Cu alloy after being co-cultured with *S. mutans* and *P. gingivalis* for 24 and 72 h (%)

Sample	*S. mutans*		*P. gingivalis*	
	24 h	72 h	24 h	72 h
Ti−3Cu	45.0	62.8	54.5	68.6

Ti−3Cu were achieved. With the extension of cultivation time to 72 h, the antibacterial rates against *S. mutans* and *P. gingivalis* increased to 62.8% and 68.6%, respectively. The increase of antibacterial rate against *S. mutans* and *P. gingivalis* were 17.8% and 14.1%, when the cultivation time increased from 24 to 72 h.

In Figs. 6(a, b), the extensive bacteria adhered and tended to form biofilm on the CP-Ti after 24 h cultivation. A large number of live bacteria and plump cells at the division stage and maturity stage could be seen in the detailed morphologies (Figs. 6(a_1, b_1)). However, only a small amount of discretely distributed bacteria could be observed on the Ti−3Cu, as shown in Figs. 6(c, d). Some shrivelled and broken dead bacteria could be found in the detailed morphologies (Figs. 6(c_1, d_1)).

Figures 7 and 8 show the fluorescent images of *S. mutans* and *P. gingivalis* after the cultivation at 37 °C for 24 and 72 h. After the cultivation for 24 h, a large number of viable bacteria were distributed on the CP-Ti sample, while the bacteria distributed on the Ti−3Cu was almost completely dead. With the extension of incubation time from 24 to 72 h, the proportion of live bacteria on the CP-Ti decreased slightly, while the proportion of dead bacteria on the Ti−3Cu increased rapidly. The bactericidal ability on the Ti−3Cu alloy delivered more pronounced over time further.

4 Discussion

The present study has found that the microstructure of the hypoeutectic Ti−3Cu alloy is composed of α-Ti matrix and nanometric Ti_2Cu precipitates (Fig. 1), and the microscale electric fields are triggered between α-Ti matrix and intermetallic particles Ti_2Cu when the Ti−3Cu samples are immersed in physiological solution. Both the polarization curves and impedance spectrum results have identified that the Ti−3Cu alloy delivers superior corrosion resistance than the

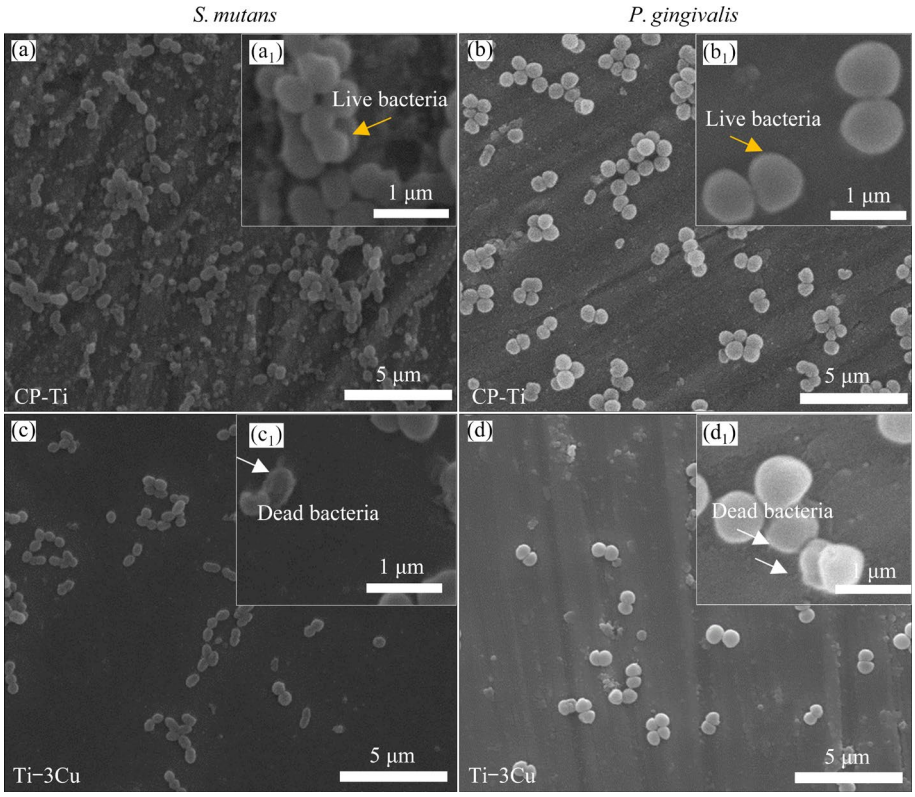

Fig. 6 SEM morphologies of *S. mutans* and *P. gingivalis* on surface of CP-Ti and Ti−3Cu alloys after 24 h co-culture (The yellow arrows show live bacteria, and the white arrows show dead bacteria)

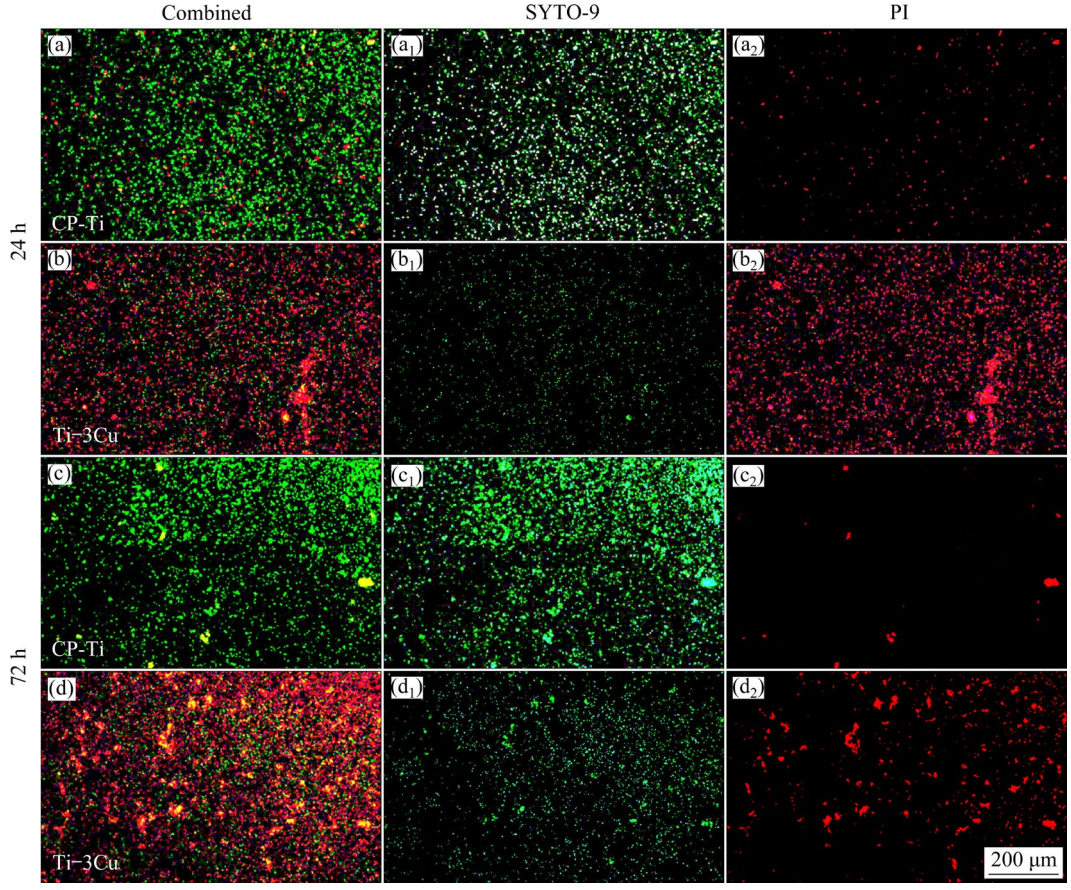

Fig. 7 Fluorescent images of *S. mutans* on CP-Ti and Ti−3Cu alloys after cultivation for 24 and 72 h at 37 °C (Green for live bacteria strained by SYTO-9 and red for dead bacteria strained by propidium iodide (PI))

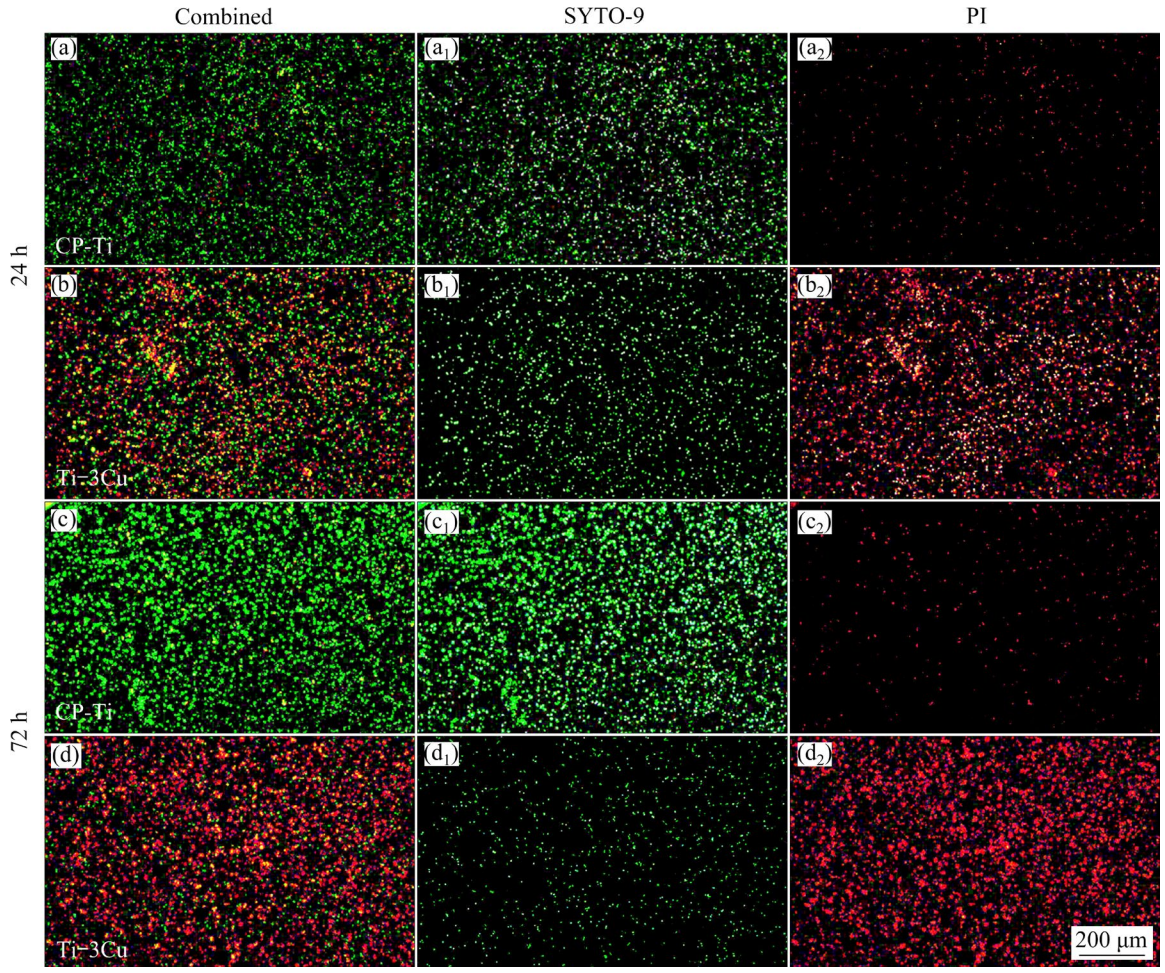

Fig. 8 Fluorescent images of *P. gingivalis* on CP-Ti and Ti−3Cu alloys after cultivation for 24 and 72 h at 37 °C (Green for live bacteria strained by SYTO-9 and red for dead bacteria strained by propidium iodide (PI))

CP-Ti. The more excellent corrosion resistance of the Ti−3Cu alloy can be attributed to the addition of Cu element, and/or to nanoprecipitates Ti_2Cu formed during manufacturing, i.e., during in-situ annealing from the laser reheating layers of previously deposited and solid material [28].

Hydrophilicity is an important factor affecting biomolecular adsorption and short-term cell adhesion [29]. Figure 3(b) demonstrated that the addition of Cu improved the surface hydrophilicity of the CP-Ti. Both the CP-Ti and the Ti−3Cu were moderately hydrophilic, and the Ti−3Cu was more plasma hydrophilic than CP-Ti. The smaller contact angle of Ti−3Cu in plasma indicated that cells tended to adhesion and growth better, which were more conducive to keep the implant stable [30]. Additionally, early prevention of bacteria adhered to implantable biomaterials in postimplantation was found to be the key to the long-term success of implants [31]. After 24 h incubation, the inhibition ring diameters of the CP-Ti was 11.8 mm, while the inhibition ring diameters of the Ti−3Cu was 13.6 mm (Fig. 4). In Fig. 6, the extensive live bacteria at the division and maturity stage adhered on the CP-Ti and tended to form biofilm, while the Ti−3Cu alloy only had some shrivelled and broken dead bacteria discretely distributed. Live and dead staining results also showed that a large number of viable bacteria distributed on the CP-Ti, while the bacteria distributed on the Ti−3Cu was almost entirely dead (Figs. 7 and 8). Under the condition of 24 h cultivation, the antibacterial activity showed a strong dependence on the addition of copper. With the addition of 3% copper, the ability to reduce bacteria adhesion and inhibit the biofilm formation was acquired. As indicated in Table 3, the antibacterial rate against *S. mutans* and *P. gingivalis* were 45.0% and 54.5% after 24 h co-culture. The

amount of released Cu^{2+} within 24 h was 53.3 μg/L in Fig. 3(a). The released Cu^{2+} from the Ti−3Cu alloy could down-regulate the expression of genes involved in bacteria adhesion, thereby inhibiting the bacterial biofilm formation [14,32]. With the extension of cultivation time from 24 to 72 h, the proportion of live bacteria on the CP-Ti decreased slightly, while the proportion of dead bacteria on the Ti−3Cu increased significantly (Figs. 7 and 8). And the antibacterial rates against *S. mutans* and *P. gingivalis* increased to 62.8% and 68.6% (Table 3). In Fig. 3(a), the Cu^{2+} released amount achieved 76.7 μg/L within 72 h. As the occurrence of α-Ti matrix and Ti_2Cu phase, the Ti−3Cu alloy could stably and enduringly release Cu^{2+}, and the release rate decreased gradually with the time prolongation. The Ti−3Cu alloy delivered a more pronounced bactericidal activity on the two kinds of bacteria over time further.

To understand the antibacterial mechanisms of Ti−3Cu alloy clearly, the generated intracellular reactive oxygen species (ROS) in bacteria cells was analysed in Fig. 9. After 24 h cultivation, intracellular ROS was detected on the Ti−3Cu alloy. Moreover, the ROS expression against *S. mutans* was more obvious, which means that the presence of both α-Ti and nanoscale Ti_2Cu in the Ti−3Cu alloy caused high intracellular super oxide levels. Furthermore, the bacteria can be dyed in red only when the cell membrane of bacteria was damaged, which means that the cell membrane of extensive bacteria was broken. Detailed morphology in Fig. 6 also confirmed that there were broken cell membranes on the Ti−3Cu after 24 h co-culture. The antibacterial mechanism might be achieved by destroying the permeability of bacterial membrane structure and making the intracellular matrix flow out and protein leakage [14].

Figure 10 illustrates the schematic diagram of generated oxidative stress within the bacteria, when the bacteria co-cultured with the Ti−3Cu alloy. The existence of galvanic corrosion between Ti_2Cu precipitates and titanium matrix, and the antibacterial performance of Ti−Cu alloy are related to the preferential release of Cu^{2+} [33]. Due to the uniform distribution of nano-scale Ti_2Cu, the potential difference between α-Ti matrix and Ti_2Cu promotes the formation of numerous micro-galvanic couples on the Ti−3Cu, resulting in electron transfer in the surrounding environment. When *S. mutans* or *P. gingivalis* contact with the Ti−3Cu alloy directly, the electron transfer on the bacteria cell membranes will be disrupted by the electron transfer on the Ti−3Cu alloy, and bacterial respiration will be interfered [34]. In addition, *S. mutans* can trigger aerobic metabolism, the part of the electrons maybe entry bacterial cells and react with O_2 and H_2O to form abundant OH^-, O_2^-

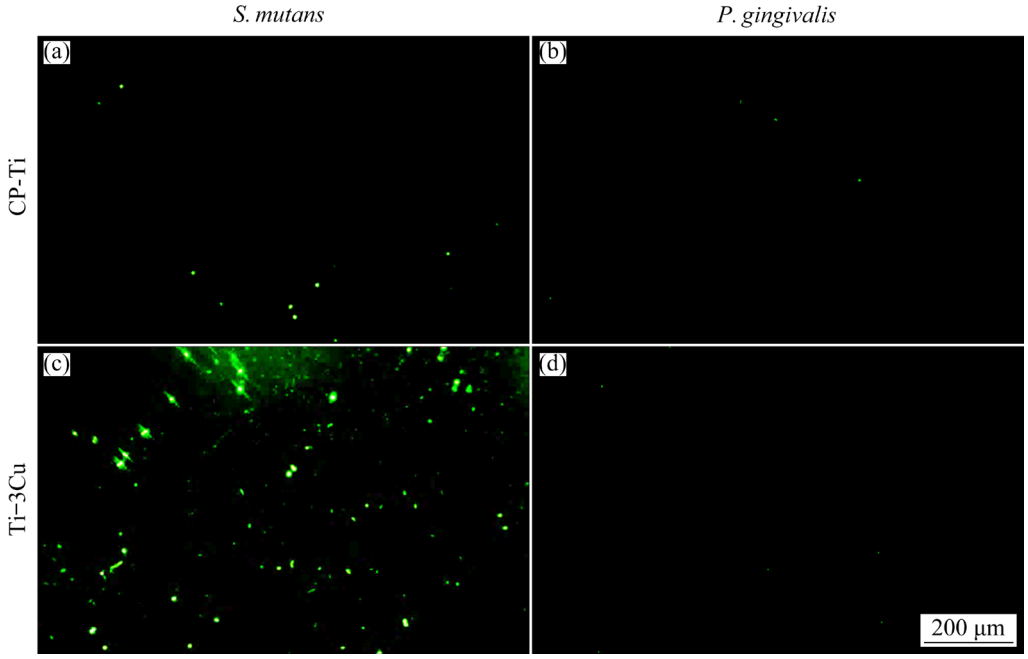

Fig. 9 Fluorescence intracellular ROS staining results of adherent *S. mutans* and *P. gingivalis* on surface of CP-Ti and Ti−3Cu after 24 h cultivation

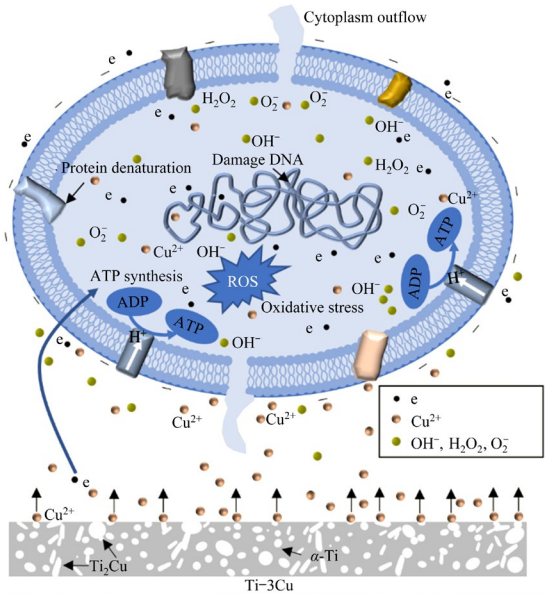

Fig. 10 Schematic diagram showing possible antibacterial mechanisms of Ti−3Cu alloy generating oxidative stress within bacteria

and H_2O_2 [34], eventually leading to excessive ROS content [35]. The specific reaction formulas are shown in Eqs. (2)−(5) [34,36]. This phenomenon is called oxidative stress [37]. High intracellular super oxide levels can generate broken cell membranes and protein leakage, rapidly killing microorganisms [38,39]. ROS can kill bacteria via damaging its cell membranes, DNA, proteins, etc [40,41]. In Figs. 6 and 9, high intracellular superoxide levels and broken cell membranes are found after 24 h cultivation. In addition, among the reactive oxygen species, OH^- is highly reactive, and excess OH^- can cause significant damage to bacterial proteins, lipids, and DNA [42].

$$H_2O+e\rightarrow \bullet H+OH^- \quad (2)$$

$$2H_2O+2e\rightarrow H_2+2OH^- \quad (3)$$

$$O_2+2e\rightarrow O_2^- \quad (4)$$

$$2O_2^-+2H^+\rightarrow H_2O_2+O_2 \quad (5)$$

The lethal process of ROS can be divided into exogenous ROS and endogenous ROS. Exogenous ROS is suitable for both *S. mutans* and *P. gingivalis*, and Cu^{2+} damages the permeability of the bacteria membrane, which can cause severe morphological and structural injuries and finally lead to the cellular materials leakage, such as proteins and sugars. Endogenous ROS is only suitable for *S. mutans* with internal respiratory chain. Cu^{2+} disrupts the activity of mitochondrial respiratory chains and superoxide anion leaks from the mitochondria, thus inhibiting cell respiration, producing high level of ROS, and suppressing the growth of bacteria [43]. With the combined action of exogenous ROS and endogenous ROS, intracellular superoxide levels in *S. mutans* on the Ti−3Cu are more significant than those of *P. gingivalis*.

The Ti−3Cu alloy prepared via SLM fulfils several key purposes. First, the supersaturated Cu is dissolved into *α*-Ti matrix and the uniformly distributed in-situ nano-precipitate is obtained in the Ti−3Cu alloy upon rapid solidification. Second, the uniformly distributed nanoscale Ti_2Cu particles not only improves the electrochemical performance, but also continuously releases Cu^{2+} through the micro-galvanic couples between *α*-Ti and Ti_2Cu. On the one hand, the released Cu^{2+} can inhibit bacterial adhesion. On the other hand, the bacteria are upset by the electron exchange in the micro-galvanic couples, producing ROS mechanism and killing bacteria. Also, the Ti−3Cu alloy prepared by SLM has good hydrophilicity, which is conducive to the adhesion and growth of human cells when it is used as implants.

5 Conclusions

(1) In the rapid cooling process of SLM, the high solubility of Cu was able to dissolve into the *α*-Ti matrix, and the uniformly distributed Ti_2Cu nanoprecipitates were formed in-situ in the Ti−3Cu alloy. These Ti_2Cu nanoprecipitates eventually reduced the corrosion. The charge transfer resistance of the Ti−3Cu alloy was doubled that of the CP-Ti.

(2) The Ti−3Cu alloy provided good antibacterial properties by inhibiting the formation of biofilms. The bactericidal activity increased with the prolongation of co-culture time. When the exposure time towards *S. mutans* and *P. gingivalis* were extended from 24 to 72 h, the antibacterial rate of the Ti−3Cu alloy increased by 17.8% and 14.1%, respectively.

(3) The electron transfer caused by the micro-galvanic couples on the Ti−3Cu alloy could interfere with the electron transport in the bacterial cells, inducing endogenous and exogenous ROS. High intracellular super oxide levels damaged the

bacterial proteins, lipids, and DNA, eventually leading to the bacteria membrane rupture and protein leakage.

CRediT authorship contribution statement

Meng-zhen ZHU: Conceptualization, Methodology, Writing − Original draft; **Jing-lei MIAO:** Software, Formal analysis; **Xiong-wen ZHOU:** Methodology, Validation, Resources, Visualization; **Er-lin ZHANG:** Investigation, Writing − Review & editing; **Zhi-lin LIU:** Writing − Review & editing; **Hai-lin YANG:** Writing − Review & editing, Supervision, Project administration.

Declaration of competing interest

The authors declare that they have no known competing financial interests or personal relationships that could have appeared to influence the work reported in this paper.

Acknowledgments

This work was financially supported by the National Natural Science Foundation of China (No. 51404302), the Natural Science Foundation of Hunan Province, China (Nos. 2020JJ4732, 2022JJ30897), and the Natural Science Foundation of Changsha City, China (No. kq2202430).

References

[1] LIU Li-nan, ZHANG Xiao-hui, LIU Hang-hang, LI Ke-han, WU Qiong-hui, LIU Yao, LUO En. Osteogenesis differences around titanium implant and in bone defect between jaw bones and long bones [J]. Journal of Craniofacial Surgery, 2020, 31: 2193−2198.

[2] YU Ai-hua, XU Wei, LU Xin, TAMADDON M, LIU Bo-wen, TIAN Shi-wei, ZHANG Ce, MUGHAL M A, ZHANG Jia-zhen, LIU Chao-zong. Development and characterizations of graded porous titanium scaffolds via selective laser melting for orthopedics applications [J]. Transactions of Nonferrous Metals Society of China, 2023, 33: 1755−1767.

[3] BRUNI S, MARTINESI M, STIO M, TREVES C, BACCI T, BORGIOLI F. Effects of surface treatment of Ti−6Al−4V titanium alloy on biocompatibility in cultured human umbilical vein endothelial cells [J]. Acta Biomaterialia, 2005, 1: 223−234.

[4] HOSEINI M, BOCHER P, SHAHRYARI A, AZARI F, SZPUNAR J A, VALI, H. On the importance of crystallographic texture in the biocompatibility of titanium based substrate [J]. Journal of Biomedical Materials Research Part A, 2014, 102: 3631−3638.

[5] KAWASE M, HAYASHI T, ASAKURA M, TOMINO M, MIEKI A, KAWAI T. Proliferation of mouse fibroblast-like and osteoblast-like cells on pure titanium films manufactured by electron beam melting [J]. Cell Biology International, 2016, 40: 1116−1122.

[6] SHIRAISHI N, MASUMOTO H, TAKAHASHI K, TENKUMO T, ANADA T, SUZUKI O, OGAWA T, SASAKI K. Histomorphometric assessments of peri-implant bone around Ti−Nb−Sn alloy implants with low Young's modulus [J]. Dental Materials Journal, 2020, 39: 148−153.

[7] FOWLER L, JANSON O, ENGQVIST H, NORGREN S, ÖHMAN-MÄGI C. Antibacterial investigation of titanium-copper alloys using luminescent *Staphylococcus epidermidis* in a direct contact test [J]. Materials Science and Engineering C, 2019, 97: 707−714.

[8] JUNTER G A, THÉBAULT P, LEBRUN L. Polysaccharide-based antibiofilm surfaces [J]. Acta Biomaterialia, 2016, 30: 13−25.

[9] WANG Yang-gang, LI Hao-yang, YUAN Xiao-yan, JIANG Yan-bin, XIAO Zi-an, LI Zhou. Review of copper and copper alloys as immune and antibacterial element [J]. Transactions of Nonferrous Metals Society of China, 2022, 32: 3163−3181.

[10] LIU Jie, ZHANG Xin-xin, WANG Hong-ying, LI Fang-bing, LI Mu-qin, YANG Ke, ZHANG Er-lin. The antibacterial properties and biocompatibility of a Ti−Cu sintered alloy for biomedical application [J]. Biomedical Materials, 2014, 9: 025013.

[11] ZHANG Er-lin, LI Fang-bing, WANG Hong-ying, LIU Jie, WANG Chun-min, LI Mu-qin, YANG Ke. A new antibacterial titanium-copper sintered alloy: Preparation and antibacterial property [J]. Materials Science and Engineering C, 2013, 33: 4280−4287.

[12] XU Bo-fan, NI Hong-wei, XIONG Ping-yuan, XIONG Juan, DAN Zhi-gang. Microstructure and antibacterial property of stainless steel implanted by Cu ions [J]. Transactions of Nonferrous Metals Society of China, 2004, 14: 328−331.

[13] LIU Heng-quan, PAN Chang-jiang, LIU Yao-hao, HUANG Nan. An inorganic coating and flexible regulating in situ of stent endothelialization by the controllable ion releasing [J]. Materials Research Bulletin, 2018, 107: 189−193.

[14] LIU Rui, TANG Yu-long, ZENG Li-lan, ZHAO Ying, MA Zheng, SUN Zi-qing, XIANG Liang-bi, REN Ling, YANG Ke. In vitro and in vivo studies of anti-bacterial copper-bearing titanium alloy for dental application [J]. Dental Materials, 2018, 34: 1112−1126.

[15] MA Zheng, REN Ling, LIU Rui, YANG Ke, ZHANG Yu, LIAO Zhen-hua, LIU Wei-qiang, QI Min, MISRA R. Effect of heat treatment on Cu distribution, antibacterial performance and cytotoxicity of Ti−6Al−4V−5Cu alloy [J]. Journal of Materials Science & Technology, 2015, 31: 723−732.

[16] SHIRAI T, TSUCHIYA H, SHIMIZU T, OHTANI K, ZEN Y, TOMITA K. Prevention of pin tract infection with titanium-copper alloys [J]. Journal of Biomedical Materials Research Part B, 2009, 91B: 373−380.

[17] CAMPOCCIA D, MONTANARO L, ARCIOLA C R. The significance of infection related to orthopedic devices and issues of antibiotic resistance [J]. Biomaterials, 2006, 27: 2331−2999.

[18] MA Chen-xu, ZHU Meng-zhen, WANG Jian-ying, ZHOU Xiong-wen, XING Hai-xia, JI Shou-xun, YANG Hai-lin. Mechanisms of improving the mechanical and antibacterial

properties of Ti−3wt.%Cu alloys [J]. Materials Letters, 2022, 319: 132263.

[19] BAO Mian-mian, LIU Ying, WANG Xiao-yan, YANG Lei, LI Sheng-yi, REN Jing, QIN Gao-wu, ZHANG Er-lin. Optimization of mechanical properties, biocorrosion properties and antibacterial properties of wrought Ti−3Cu alloy by heat treatment [J]. Bioactive Materials, 2018, 3: 28−38.

[20] YANG Hai-lin, ZHU Meng-zhen, WANG Jian-ying, MA Chen-xu, ZHOU Xiong-wen, XING Hai-xia, ZHANG Er-lin, JI Shou-xun. Optimization of mechanical and antibacterial properties of Ti−3wt.%Cu alloy through cold rolling and annealing [J]. Rare Metals, 2022, 41: 610−620.

[21] SING S L, AN J, YEONG W Y, WIRIA F E. Laser and electron-beam powder-bed additive manufacturing of metallic implants: A review on processes, materials and designs [J]. Journal of Orthopaedic Research, 2016, 34: 369−385.

[22] WANG Jian-ying, ZOU Jian-peng, YANG Hai-lin, ZHANG Li-jun, LIU Zhi-lin, DONG Xi-xi, JI Shou-xun. Exceptional strength-ductility synergy of additively manufactured CoCrNi medium-entropy alloy achieved by lattice defects in heterogeneous microstructures [J]. Journal of Materials Science & Technology, 2022, 127: 61−70.

[23] JU Jiang, LI Jing-jing, JIANG Min, LI Meng-ya, YANG Li-xiang, WANG Kai-ming, YANG Chao, KANG Mao-dong, Wang Jun. Microstructure and electrochemical corrosion behavior of selective laser melted Ti−6Al−4V alloy in simulated artificial saliva [J]. Transactions of Nonferrous Metals Society of China, 2021, 31: 167−177.

[24] ZHANG Du-yao, QIU Dong, GIBSON M A, ZHENG Yu-feng, FRASER H L, STJOHN D H, EASTON M A. Additive manufacturing of ultrafine-grained high-strength titanium alloys [J]. Nature, 2019, 576: 91−95.

[25] WANG Xiao-lan, LIU Shao-xiang, LI Mei, YU Peng, CHU Xiao, LI Li-hua, TAN Guo-xin, WANG Ying-jun, CHEN Xiao-feng, ZHANG Yu, NING Cheng-yun. The synergistic antibacterial activity and mechanism of multicomponent metal ions-containing aqueous solutions against *Staphylococcus aureus* [J]. Journal of Inorganic Biochemistry, 2016, 163: 214−220.

[26] NING Cheng-yun, WANG Xiao-lan, LI Li-hua, ZHU Ye, LI Mei, YU Peng, ZHOU Lei, ZHOU Zheng-nan, CHEN Jun-qi, TAN Guo-xin, ZHANG Yu, WANG Ying-jun, MAO Chuan-bin. Concentration ranges of antibacterial cations for showing the highest antibacterial efficacy but the least cytotoxicity against mammalian cells: Implications for a new antibacterial mechanism [J]. Chemical Research in Toxicology, 2015, 28: 1815−1822.

[27] OSÓRIO W R, CREMASCO A, ANDRADE P N, GARCIA A, CARAM R. Electrochemical behavior of centrifuged cast and heat treated Ti−Cu alloys for medical applications [J]. Electrochimica Acta, 2010, 55: 759−770.

[28] OSÓRIO W R, SPINELLI J E, FERREIRA I L, GARCIA A. The roles of macrosegregation and of dendritic array spacings on the electrochemical behavior of an Al−4.5wt.%Cu alloy [J]. Electrochimica Acta, 2007, 52: 3265−3273.

[29] MAS-MORUNO C, GARRIDO B, RODRIGUEZ D, RUPEREZ E, GIL F J. Biofunctionalization strategies on tantalum-based materials for osseointegrative applications [J]. Journal of Materials Science: Materials in Medicine, 2015, 26: 1−12.

[30] CHEN Meng, ZAMORA P O, SOM P, PEÑA L A, OSAKI S. Cell attachment and biocompatibility of polytetrafluoro-ethylene (PTFE) treated with glow-discharge plasma of mixed ammonia and oxygen [J]. Journal of Biomaterials Science−Polymer Edition, 2003, 14: 917−935.

[31] LI Pei-yuan, TONG Zhang-fa, HUO Li-ni, YANG Fang, SU Wei. Antibacterial and biological properties of biofunctionalized nanocomposites on titanium for implant application [J]. Journal of Biomaterials Applications, 2016, 31: 205−214.

[32] LI Yang, LIU Li-na, WAN Peng, ZHAI Zan-jing, MAO Zhen-yang, OUYANG Zheng-xiao, YU De-gang, SUN Qi, TAN Li-li, REN Ling, ZHU Zhen-an, HAO Yong-qiang, QU Xin-hua, YANG Ke, DAI Ke-rong. Biodegradable Mg−Cu alloy implants with antibacterial activity for the treatment of osteomyelitis: *In vitro* and *in vivo* evaluations [J]. Biomaterials, 2016, 106: 250−263.

[33] LIU Jie, LI Fang-bing, LIU Cong, WANG Hong-ying, REN Bao-rui, YANG Ke, ZHANG Er-lin. Effect of Cu content on the antibacterial activity of titanium-copper sintered alloys [J]. Materials Science and Engineering C, 2014, 35: 392−400.

[34] OUYANG Si-hui, ZHENG Kai, ZHANG Wei-dong, CHEN Wen-juan, LIU Yong. Microscale electric fields induced by galvanically coupled Ti−Mg metal-metal composites promote antibacterial activity [J]. Materialia, 2020, 9: 100621.

[35] LU Ji, WANG Yue, JIN Min, YUAN Zhi-guo, BOND P, GUO Jian-hua. Both silver ions and silver nanoparticles facilitate the horizontal transfer of plasmid-mediated antibiotic resistance genes [J]. Water Research, 2020, 169: 115229.

[36] JAEGER C D, BARD A J. Spin trapping and electron spin resonance detection of radical intermediates in the photodecomposition of water at titanium dioxide particulate systems [J]. The Journal of Physical Chemistry, 1979, 83: 3146−3152.

[37] DHARMARAJA A T. Role of reactive oxygen species (ROS) in therapeutics and drug resistance in cancer and bacteria [J]. Journal of Medicinal and Chemistry, 2017, 60: 3221−3240.

[38] CIRCU M L, AW T Y. Reactive oxygen species, cellular redox systems, and apoptosis [J]. Free Radical Biology and Medicine, 2010, 48: 749−762.

[39] LIAO Juan, ZHU Zhi-min, MO An-chun, LI Lei, ZHANG Jing-chao. Deposition of silver nanoparticles on titanium surface for antibacterial effect [J]. International Journal of Nanomedicine, 2010, 5: 261−267.

[40] XI Ju-qun, WEI Gen, AN Lan-fang, XU Zhuo-bin, XU Zhi-long, FAN Lei, Gao Li-zeng. Copper/carbon hybrid nanozyme: Tuning catalytic activity by the copper state for antibacterial therapy [J]. Nano Letters, 2020, 19: 7645−7654.

[41] HUANG Bo, TAN Lei, LIU Xiang-mei, LI Jun, WU Shui-lin. A facile fabrication of novel stuff with antibacterial property and osteogenic promotion utilizing red phosphorus and near-infrared light [J]. Bioactive Materials, 2019, 4: 17−21.

[42] DHAR H P, HOWELL D W, BOCKRIS J O'. The use of *in situ* electrochemical reduction of oxygen in the diminution of adsorbed bacteria on metals in seawater [J]. Journal of the Electrochemical Society, 1982, 129: 2178−2182.
[43] LI Mei, MA Zheng, ZHU Ye, XIA Hong, YAO Meng-yu, CHU Xiao, WANG Xiao-lan, YANG Ke, YANG Ming-ying, ZHANG Yu, MAO Chuan-bin. Toward a molecular understanding of the antibacterial mechanism of copper-bearing titanium alloys against *staphylococcus aureus* [J]. Advanced Healthcare Materials, 2016, 5: 557−566.

选区激光熔化成形 Ti−3Cu 合金的耐腐蚀性能及抗菌性能

朱梦真[1]，苗惊雷[2]，周雄文[3]，张二林[4]，刘峙麟[5]，杨海林[1]

1. 中南大学 粉末冶金国家重点实验室，长沙 410083；
2. 中南大学 湘雅第三医院，长沙 410013；
3. 中南大学 湘雅医院 口腔医学中心 修复科，长沙 410008；
4. 东北大学 材料科学与工程学院 材料各向异性与织构教育部重点实验室，沈阳 110819；
5. 中南大学 机电工程学院 轻合金研究所，长沙 410083

摘　要：采用电化学实验和多种抗菌特性对选区激光熔化成形 Ti−3Cu 合金的耐腐蚀性能和抗菌性能进行评价。结果表明，Ti−3Cu 合金的电荷转移电阻为 4.89×10^5 Ω·cm^2，约为 CP-Ti 合金电荷转移电阻的 2 倍。Ti−3Cu 合金对变形链球菌和牙龈卟啉单胞菌的抑菌率分别为 45.0%和 54.5%，且抑菌率随共培养时间的延长分别增加到 62.8%和 68.6%。原位生成的纳米 Ti_2Cu 析出相均匀分布在 Ti−3Cu 合金基体中，提升了合金的耐腐蚀性能。此外，α-Ti 基体和 Ti_2Cu 反应形成的微电偶是抗菌性能增强的主要原因。

关键词：选区激光熔化；Ti−3Cu 合金；显微组织；耐腐蚀性能；抗菌性能

(Edited by Bing YANG)